NMR IN BIOMEDICINE
NMR Biomed. 2004;**17**:554–568
Published online in Wiley InterScience (www.interscience.wiley.com). DOI:10.1002/nbm.937

Functional mapping of neural pathways in rodent brain *in vivo* using manganese-enhanced three-dimensional magnetic resonance imaging

Takashi Watanabe, Jens Frahm and Thomas Michaelis*

Biomedizinische NMR Forschungs GmbH am Max-Planck-Institut für biophysikalische Chemie, Göttingen, Germany

Received 12 March 2004; Revised 1 October 2004; Accepted 1 October 2004

ABSTRACT: This work presents three-dimensional MRI studies of rodent brain *in vivo* after focal and systemic administration of $MnCl_2$. Particular emphasis is paid to the morphology and dynamics of Mn^{2+}-induced MRI signal enhancements, and the physiological mechanisms underlying cerebral Mn^{2+} uptake and distribution. It turns out that intravitreal and intrahippocampal injections of $MnCl_2$ emerge as useful tools for a delineation of major axonal connections in the intact central nervous system. Subcutaneous administrations may be exploited to highlight regions involved in fundamental brain functions such as the olfactory bulb, inferior colliculus, cerebellum and hippocampal formation. Specific insights into the processes supporting cerebral Mn^{2+} accumulation may be obtained by intraventricular $MnCl_2$ injection as well as by pharmacologic modulation of, for example, hippocampal function. Taken together, Mn^{2+}-enhanced MRI opens new ways for mapping functioning pathways in animal brain *in vivo* with applications ranging from assessments of transgenic animals to follow-up studies of animal models of human brain disorders. Copyright © 2004 John Wiley & Sons, Ltd.

KEYWORDS: magnetic resonance imaging; manganese; neural tract tracer; contrast agent; brain morphology; brain function; hippocampus; visual pathway

INTRODUCTION

Since the pioneering work of Koretsky and coworkers,[1,2] the use of Mn^{2+} ions has attracted growing attention both in the MRI community and among researchers in neuroscience. Particular interest in the use of Mn^{2+} stems from its potential as an MRI contrast agent for functional mapping of animal brain *in vivo*. Exploring various administration routes the technique has been optimized for a large number of brain systems and a variety of vertebrates (e.g. see other papers in this volume).

In principle, the approach relies upon the fact that Mn^{2+} can be taken up by excitable neurons as an analog to Ca^{2+} through voltage-gated divalent cation channels.[3,4] For example, in cultured cerebellar granule cells, the entry of extracellular Mn^{2+} via Ca^{2+}-permeant channels has been demonstrated using fluorescence quenching of intracellular indicator dyes after cellular stimulation either by depolarization using a high potassium concentration or by glutamatergic agonists.[5] These data support the notion that the uptake of extracellular Mn^{2+} by a neuron is directly coupled to its physiologic activity and function.

Here, we review recent *in vivo* MRI findings of Mn^{2+}-induced signal enhancements in the brain of behaving mice and rats which have been obtained 2–72 hours after focal or systemic administration of a single dose of $MnCl_2$.

**Correspondence to:* T. Michaelis, Biomedizinische NMR Forschungs GmbH, 37070 Göttingen, Germany.
E-mail: tmichae@gwdg.de

Abbreviations used: APV, DL-2-amino-5-phosphonovaleric acid; BBB, blood–brain barrier; CA1–CA4, hippocampal subfields; Ce, cerebellum; CNR, contrast-to-noise ratio; CNS, central nervous system; CP, choroid plexus; CSF, cerebrospinal fluid; DG, dentate gyrus; Fi, fimbria; FLASH, fast low angle shot; Fx, precommissural fornix; GL, granule cell layer; Hb, habenula; HF, hippocampal formation; Hi, hilus; IC, inferior colliculus; IP, interpeduncular nucleus; ISF, interstitial fluid; L, stratum lucidum; LGN, lateral geniculate nucleus; LSD, dorsolateral septal nucleus; MRI, magnetic resonance imaging; OB, olfactory bulb; ON, optic nerve; OPN, olivary pretectal nucleus; OT, optic tract; Pi, pineal gland; Pit, pituitary gland; Ret, retina; ROI, region-of-interest; S, subiculum; SC, superior colliculus; SCN, suprachiasmatic nucleus; SD, standard deviation; SNR, signal-to-noise ratio; SP, stratum pyramidale; TSN, triangular septal nucleus; VHC, ventral hippocampal commissure.

MATERIALS AND METHODS

Animals and MRI

All studies were performed in accordance with German animal protection laws and approved by the responsible governmental authority. MRI was carried out at 2.35 T using a MRBR 4.7/400 mm magnet (Magnex Scientific, Abingdon, UK) equipped with B-GA20 gradients (200 mm inner diameter, 100 mT m^{-1} maximum strength) and driven by a DBX system (Bruker Biospin, Ettlingen, Germany).

For *in vivo* MRI the animals were kept under anesthesia using 0.2–1.5% halothane in a 7:3 mixture of N_2O and O_2. After being relaxed, the animals were intubated with a purpose-built endotracheal tube, and artificially ventilated with an animal respirator. Rats and mice were placed in a supine and prone position, respectively, with their heads firmly fixed in a purpose-built stereotaxic device. The rectal body temperature was maintained constant at $37 \pm 1\,^{\circ}C$ using heated water blankets. After each measurement the animals were recovered from anesthesia and returned to their cages with free access to food and water.

For rats radiofrequency excitation and signal reception were accomplished with use of a birdcage coil (154 mm inner diameter) and a saddle-shaped surface coil (40 mm diameter), respectively. Mice were studied with a Helmholtz excitation coil (100 mm diameter) and an elliptical surface coil (20 mm anterior–posterior, 12 mm left–right) for signal reception.

Image acquisitions were based on a T_1-weighted gradient-echo MRI sequence (radiofrequency-spoiled three-dimensional FLASH) yielding a spatial resolution ranging from $195 \times 195 \times 125\,\mu m^3$ for rats to an isotropic resolution of 117 μm for mice.[6] Explicit values are given in the figure captions. For a more detailed description of experimental methods, readers are referred to the original publications.[7–10]

Manganese administration

The visual pathway of rats was studied using a 5 min injection of an aqueous solution of $MnCl_2$ (0.1 μl, 1000 mM) following experimental procedures described elsewhere.[7] Briefly, injections were performed under anesthesia by inserting a needle into the vitreous body of the left eye with the aid of a microscope. Proper placement of the needle was verified by observing the magnified image of the tip through the lens of the animal's eye. After 15 min the needle was slowly withdrawn to minimize the loss of $MnCl_2$ from leakage at the injection site.

The hippocampal system of C57BL/6J mice was studied with use of stereotaxic bilateral microinjections of $MnCl_2$ (0.25 μl, 5–200 mM) into the posterior hippocampal formation.[10] Similarly, mouse studies of the cerebral uptake and distribution of Mn^{2+} from the CSF employed stereotaxic injections of $MnCl_2$ (0.25 μl, 5 mM) into the left lateral ventricle. Systemic administrations in mice were accomplished by means of subcutaneous injections of $MnCl_2$ (5 ml/kg body weight, 20 mM).[8]

Data analysis

For image analysis anatomic cross-sections were obtained by multiplanar reconstructions from the original three-dimensional (3D) MRI data sets. Quantitative evaluations of the signal-to-noise ratio (SNR), here defined as the MRI signal intensity divided by the standard deviation of the noise, were performed using software supplied by the manufacturer. Standardized regions-of-interest (ROI) were selected in close accordance to resolved anatomic structures.

RESULTS

Intravitreal manganese administration

Figure 1 shows a pronounced anterograde Mn^{2+} enhancement of retinal projections in rat brain after injection of an aqueous $MnCl_2$ solution into the left vitreous body.[7] The images represent selected sections from a 3D MRI data set obtained 24 h after injection. They result in a clear delineation of the retina, the axonal tract and terminal fields including the suprachiasmatic nuclei. Because the vitreous body serves as a closed reservoir for Mn^{2+} ions, sufficient amounts of $MnCl_2$ can be administered near to retinal neurons without damaging their cellular membrane integrity. Therefore, the observed MRI signal enhancement may be assigned to the neuronal uptake of Mn^{2+} ions rather than to their diffusion into the intracellular space through torn neuronal membranes.

The enhancement of the rat retinal projection pathway is best delineated by maximum intensity projections shown in Fig. 2. A comparison of results obtained at various stages after injection revealed an optimal CNR and good anatomic continuity of enhanced structures at 24 h post-injection. While early data sets exhibited insufficient transport of Mn^{2+} ions beyond the optic chiasm, examinations at 48 h post-injection or later suffered from fading contrast. It should be noted, however, that the axonal terminal areas showed less decline of the Mn^{2+}-induced contrast between 24 and 72 h post-injection than the optic tract, which represents the projecting portion of the axons.

A quantitative analysis of the SNR in structures with increasing distance from the injection site confirms these observations. Table 1 summarizes SNR values for the enhanced optic nerve (nearest to the injection site), the contralateral optic tract (medial distance) and the contralateral superior colliculus (largest distance) as well as for control regions in the cortex and basal ganglia. The sequential acquisitions at different time points allowed for an estimate of the velocity of the Mn^{2+} enhancement along the projection fibers. For example, a weak but unequivocal enhancement of the superior colliculus was detected about 8 h after injection in all animals. From the 3D MRI data the length of the pathway from the optic disc to the superior colliculus was determined to be 22.5 ± 0.9 mm which results in a speed of about $2.8\,mm\,h^{-1}$ for the axonal transport of Mn^{2+} ions.

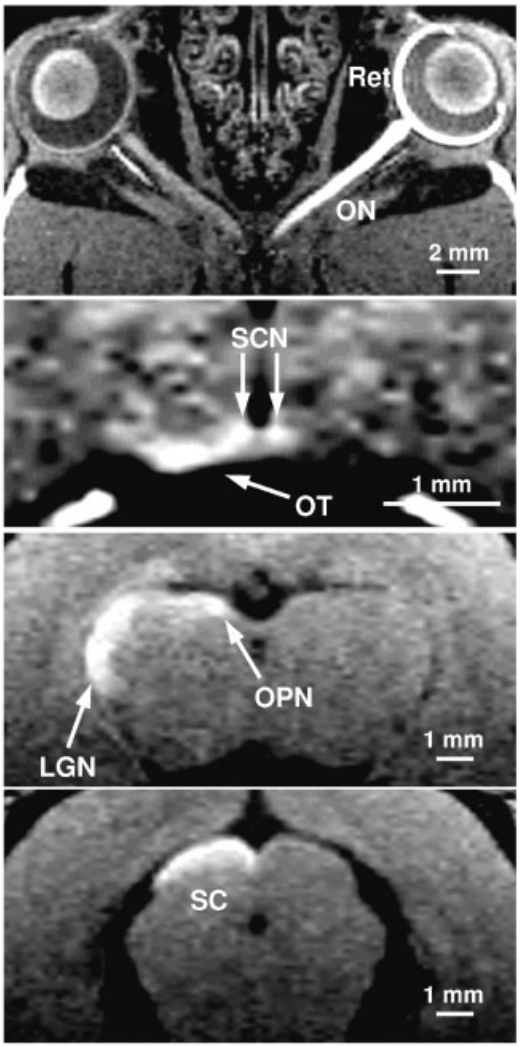

Figure 1. Manganese-induced MRI signal enhancement of the rat retinal projection pathway 24 h after injection of 0.1 µl $MnCl_2$ (1000 mM) into the left vitreous body (T_1-weighted 3D FLASH, *TR/TE* = 15/4.2 ms, 25° flip angle, $195 \times 195 \times 125\ \mu m^3$ resolution). Enhanced structures refer to the left retina (Ret), left optic nerve (ON), right optic tract (OT), right and left suprachiasmatic nucleus (SCN), right lateral geniculate nucleus (LGN), right olivary pretectal nucleus (OPN), and right superior colliculus (SC). [Adapted and reproduced from Watanbe T, Michaelis T, Frahm J. Mapping of retinal projections in the living rat using high-resolution 3D gradient-echo MRI with MN^{2+}-induced contrast. *Magn. Reson. Med*. 2001; **46**: 424–429. Copyright © 2001 John Wiley & Sons, Inc. Reprinted with permission of Wiley-Liss, Inc., a subsidiary of John Wiley & Sons, Inc.] [7]

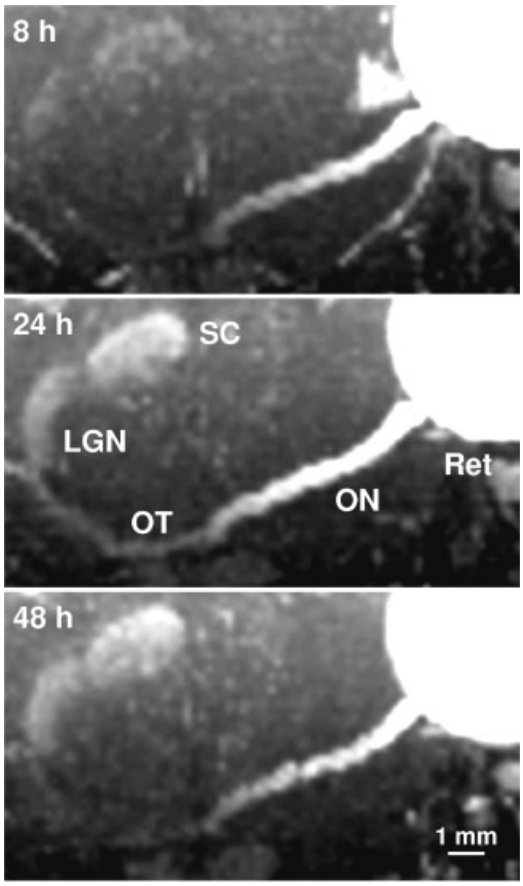

Figure 2. Maximum intensity projections of the retinal projection pathway (same animal as in Fig. 1) at (top) 8 h, (middle) 24 h and (bottom) 48 h after $MnCl_2$ injection into the left vitreous body (rostro-caudal view to minimize overlap of enhanced structures with high intensities from fat and vessels). For other parameters see Fig. 1. [Adapted and reproduced from Watanabe T, Michaelis T, Frahm J. Mapping of retinal projections in the living rat using high-resolution 3D gradient-echo MRI with MN^{2+}-induced contrast. *Magn. Reson. Med*. 2001; **46**: 424–429. Copyright © 2001 John Wiley & Sons, Inc. Reprinted with permission of Wiley-Liss, Inc., a subsidiary of John Wiley & Sons, Inc.][7]

The *in vivo* Mn^{2+} mapping of the rat visual pathway is in general agreement with the well-documented projections identified by conventional invasive methods. In rodents, the great majority of the optic nerve fibers are known to cross at the chiasm.[11] The fibers then enter the

Table 1. SNR of the rat visual pathway after intravitreous injection of 0.1 µl $MnCl_2$ (1000 mM)

Region	ROI (mm^2)	8 h ($n = 3$)	24 h ($n = 4$)	48 h ($n = 4$)	72 h ($n = 3$)
Left optic nerve	0.20	22.0 ± 0.7	25.0 ± 3.9	22.6 ± 3.1	20.1 ± 4.4
Right optic tract	0.34	18.2 ± 2.1	19.5 ± 2.0	18.9 ± 1.6	17.7 ± 1.8
Superior colliculus	0.57	26.9 ± 1.5	32.0 ± 1.9	29.1 ± 3.3	28.8 ± 3.3
Cortex	0.95	19.1 ± 1.1	18.5 ± 1.7	19.2 ± 0.8	18.4 ± 1.9
Basal ganglia	0.95	17.1 ± 0.8	16.6 ± 1.1	17.4 ± 1.1	16.9 ± 0.5

The data represent mean values ± SD averaged across animals.

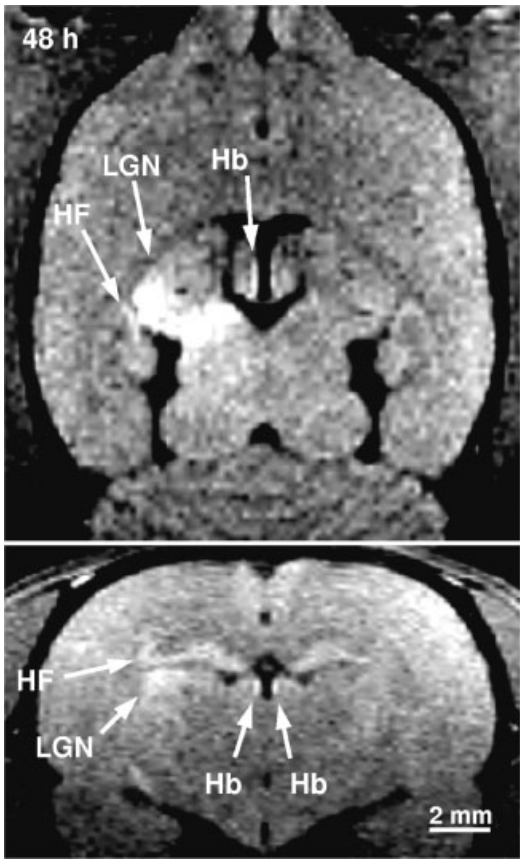

Figure 3. (Top) Manganese-induced MRI signal enhancement in a horizontal and (bottom) coronal section (same animal as in Fig. 1) at 48 h after $MnCl_2$ injection into the left vitreous body. In addition to the enhancement of the right lateral geniculate nucleus (LGN), signal increases are observed outside the visual pathway within the CA3 subregion of the right hippocampal formation (HF) and within the habenula (Hb) bilaterally. For other parameters see Fig. 1

optic tract, which projects to subcortical targets involving the lateral geniculate nucleus, the pretectal area, and the superior colliculus.[12,13] In addition, a direct retinohypothalamic projection to the suprachiasmatic nucleus has been described.[14,15] Here, a Mn^{2+} enhancement was also observed in regions outside the visual system during late phases after injection. At 48 h, Fig. 3 demonstrates unambiguous MRI signal increases in the CA3 region of the hippocampus and in the habenulae. Because a major retinal projection into these regions has not been reported, these findings suggest a high affinity of pertinent structures to Mn^{2+} ions. A corresponding accumulation of Mn^{2+} in the hippocampal formation has also been observed after systemic administration (see below).

Intrahippocampal manganese administration

The concept of Mn^{2+} as a neural tracer, which can be taken up by sensory neurons and axonally transported in brain tissue, lends itself to direct intracerebral injections. Such strategies offer the advantage that the exogenous tracer can be focally delivered to a target region. Subsequent MRI bears the potential for unraveling Mn^{2+} uptake, transport and accumulation by specific neuronal populations located deeply in the brain.

Because of its central role in episodic memory processing, the hippocampus and its projections are of key interest for functional tract tracing using Mn^{2+}-enhanced MRI. The hippocampal formation is composed of the dentate gyrus, the subfields CA1–CA4, and the subiculum.[16,17] The majority of the hippocampal extrinsic projection fibers are known to enter the white matter bundle known as fimbria before ascending and joining a midline projection pathway called fornix. Through this fimbria–fornix complex, hippocampal pyramidal cells from all CA subfields project to the septal complex.[16,18] Rodents additionally exhibit extensive commissural connections passing through a ventral hippocampal commissure located posterior to the septal area.

As demonstrated in Fig. 4 intrahippocampal injections of $MnCl_2$ induced marked MRI signal increases within the posterior hippocampal formation.[10] In comparison with data acquired 2 h post-injection, Mn^{2+}-enhanced MRI after 6 h revealed a more heterogenous and spatially distinct signal behavior within the hippocampal formation. Whereas mild signal increases are seen in CA1 and the subiculum, the pronounced enhancement in CA3 and the dentate gyrus suggests the accumulation of Mn^{2+} ions in pyramidal and granule cells, respectively.

In addition to MRI signal increases in the vicinity of the injection sites, intrahippocampal $MnCl_2$ administration led to a pronounced MRI signal enhancement of the fimbria–fornix complex. At 2 h after injection, Mn^{2+} transport beyond the level of the ventral hippocampal commissure was still incomplete. In terms of anatomic continuity, a better contrast enhancement of the efferent pathway was achieved 6 h after injection. As summarized in Fig. 5, coronal MRI sections along the hippocampo-septal projection pathway clearly highlight the projecting fiber bundles and axonal terminal areas. In fact, 3D MRI allowed for a visualization of the entire course of fibers through the fimbria up to the septal region with the ventral hippocampal commissure showing the most pronounced enhancement. Additional signal increases were observed in the septal complex at the dorsal part of the lateral septal nucleus as well as in the precommissural fornix and the trigeminal septal nucleus. More specifically, the enhancement of the fimbria at the medial position is a consequence of Mn^{2+} uptake into ammonic and subicular pyramidal cells of the posterior hippocampus and in close agreement with a previous anterograde tracing study.[20]

The SNR and CNR values for the projection pathway at the level of the ventral hippocampal commissure are summarized in Table 2. The length of the pathway from the injection site via the fimbria to the ventral hippocampal

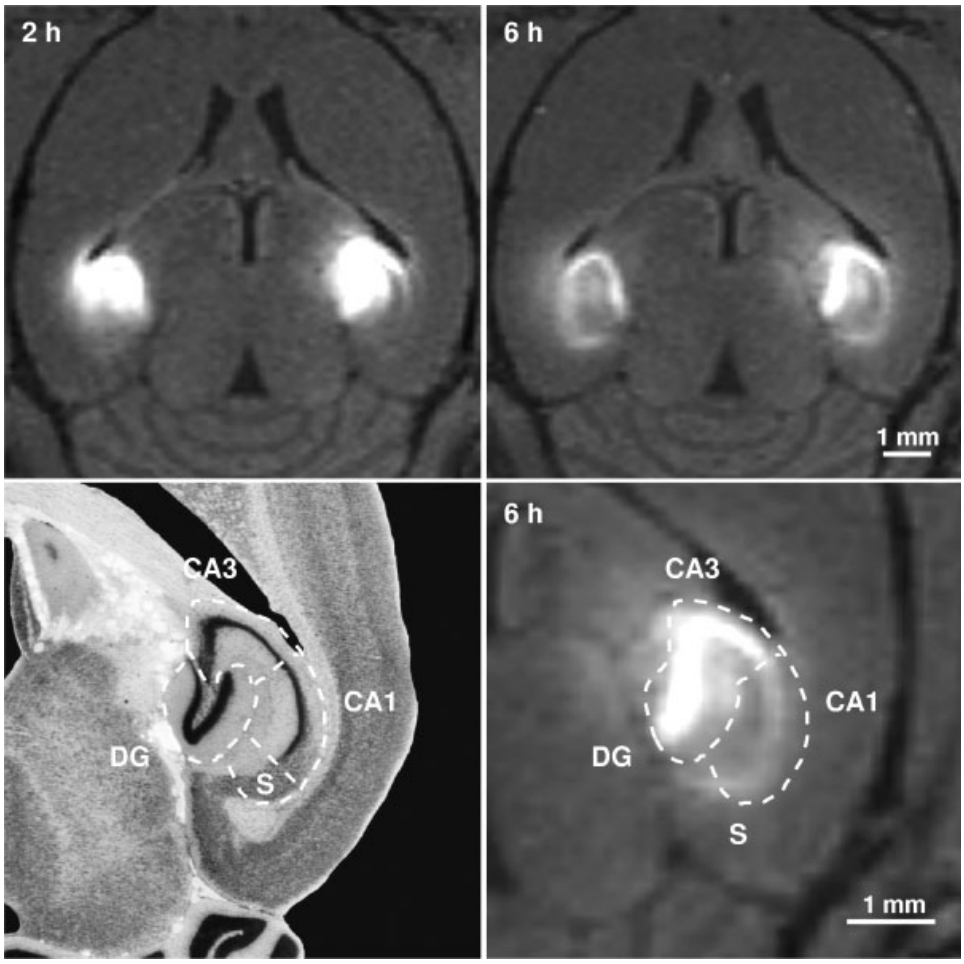

Figure 4. (Top) Manganese-induced MRI signal enhancement of the brain of a C57BL/6J mouse (left) 2 h and (right) 6 h after intrahippocampal injection of 0.25 µl of $MnCl_2$ (200 mM) in horizontal sections (T_1-weighted 3D FLASH, $TR/TE = 17/7.6$ ms, 25° flip angle, $117 \times 156 \times 156\ \mu m^3$ interpolated to 117 µm isotropic resolution). In contrast to pronounced signal increases in and around the posterior hippocampal formation early after injection, MRI at 6 h reveals a more heterogenous and spatially distinct signal behavior. (Bottom) The left hippocampal formation of a C57BL/6J mouse in (left) a histologic section (courtesy of Rosen *et al.*)[19] and (right) a corresponding MRI section 6 h after intrahippocampal $MnCl_2$ injection (magnified view of top right image). The latter demonstrates MRI signal enhancement in the dentate gyrus (DG) and CA3 subfield as well as milder signal increases in the CA1 subfield and subiculum (S). [Reprinted from *Neuroimage*, **22**; Watanabe T, Radulovic J, Spiess J, Natt O, Boretius S, Frahm J, Michaelis T. *In vivo* 3D MRI staining of the mouse hippocampal system using intrecerebral injection of $MnCl_2$; 860–867. Copyright © 2004, with permission from Elsevier.][10]

commissure was determined to be 4.3 ± 0.5 mm in both hemispheres. An evaluation of the time course of SNR increases demonstrates that 2 h are sufficient to transport Mn^{2+} ions from the posterior hippocampus to the ventral hippocampal commissure, but that-at least for a 5 mM solution of $MnCl_2$-this process has not led to a saturation of the local Mn^{2+} concentration.

Subcutaneous manganese administration

Observations of Mn^{2+}-induced MRI signal enhancements in response to a focal exposure of retinal or hippocampal neurons to $MnCl_2$ confirm the capability of Mn^{2+} ions to specifically label neuronal populations and to map connected axonal tracts. Beyond this qualitative understanding, regional differences in Mn^{2+} affinity between brain systems and even within a single system may be related to quantitative differences in brain function. Such effects should also become detectable after systemic applications of $MnCl_2$ which are expected to yield specific cerebral enhancements discernable from a non-specific 'background' MRI signal enhancement of 'less active' brain tissue. In fact, high-resolution autoradiography demonstrated Mn^{2+} ions to accumulate in the olfactory bulb, olfactory nuclei, inferior colliculi,

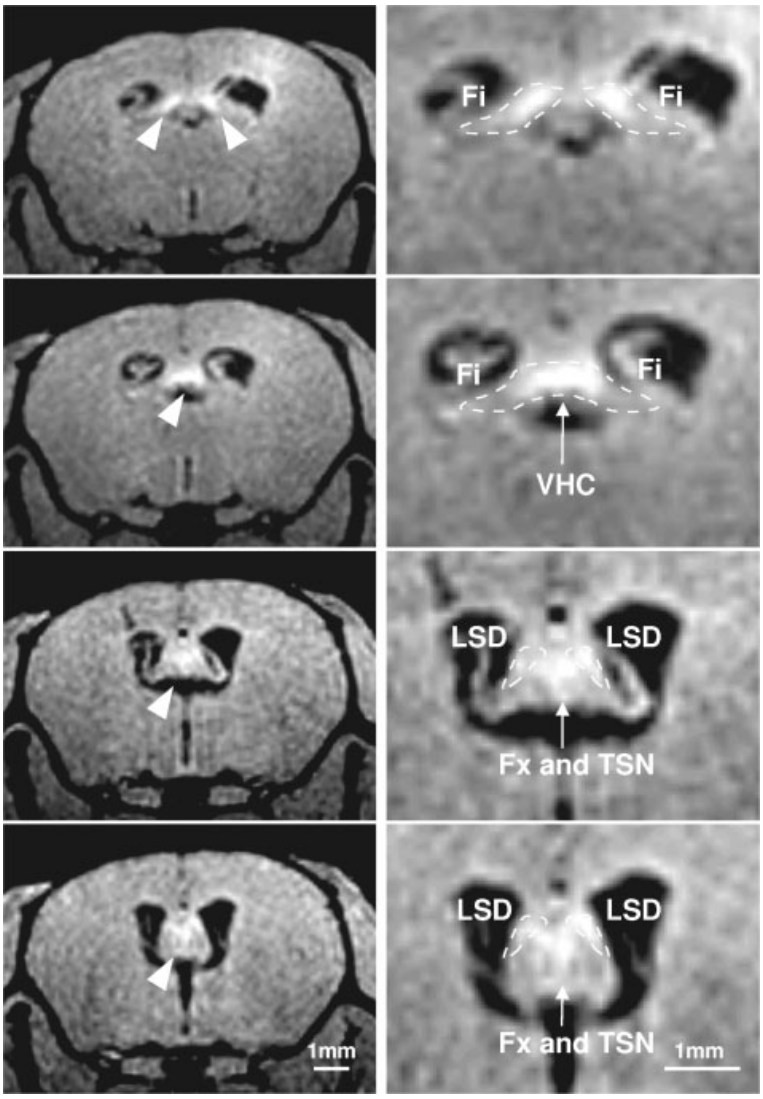

Figure 5. (Left) Manganese-induced MRI signal enhancement along the hippocampo-septal projection pathway of a C57BL/6J mouse (same animal as in Fig. 4) 6 h after intrahippocampal injection of $MnCl_2$ and (right) corresponding magnified views. Arrowheads and dashed lines indicate enhanced structures such as the medial part of the fimbria (Fi) bilaterally, the ventral hippocampal commissure (VHC), the dorsal part of the lateral septal nucleus (LSD) bilaterally, the precommissural fornix (Fx), and the triangular septal nucleus (TSN). For other parameters see Fig. 4. [Reprinted from *Neuroimage*, **22**; Watanabe T, Radulovic J, Spiess J, Natt O, Boretius S, Frahm J, Michaelis T. *In vivo* 3D MRI staining of the mouse hippocampal system using intrecerebral injection of $MnCl_2$; 860–867. Copyright © 2004, with permission from Elsevier.][10]

Table 2. SNR and CNR of the ventral hippocampal commissure and the cortex of C57BL/6J mice after intrahippocampal injection of 0.25 µl $MnCl_2$ (5 mM)

	Region	ROI (mm^2)	Control ($n=3$)	2 h ($n=4$)	6 h ($n=3$)
SNR	VHC	0.50	24.6 ± 1.2	28.9 ± 1.7*	32.1 ± 1.9**
	Cortex	0.50	20.7 ± 1.4	22.2 ± 1.0	23.8 ± 1.3*
CNR	VHC – cortex	—	3.9 ± 0.3	6.7 ± 1.0*	8.3 ± 0.8**

The data represent mean values ± SD averaged across animals; *$p < 0.05$, **$p < 0.01$ (unpaired t-test vs control).

amygdala, thalamus, hippocampal formation and cerebellum after systemic administration.[21–23] Moreover, non-MRI studies indicated that Mn^{2+} reaches the brain across the BBB and blood-CSF barrier.[24–26]

Figure 6 reveals spatially distinct short-term and long-term MRI signal enhancements in mouse brain after systemic $MnCl_2$ application.[9] For MRI, a subcutaneous route was chosen in order to provide a sustained supply of Mn^{2+} ions via a slow rate of absorption into the systemic circulation. This seems to be advantageous in terms of Mn^{2+} delivery to the brain because the transfer across the BBB is limited[24] and because the approach avoids 'first-pass' hepatic losses as the bile is the main route for the elimination of Mn^{2+} from the body.[27] At 6 h after administration (center column of Fig. 6), the choroid plexus, pineal gland and anterior pituitary gland show a pronounced enhancement. On the other hand, brain regions such as the olfactory bulb, hippocampal formation and cerebellar cortex reveal an enhancement in later examinations (right column). At 48 h, the Mn^{2+} enhancement improves the delineation of the layered structures within the cerebellum as the outer bright layer circumscribes an interior region without a substantial SNR increase. Most likely, the bright signal represents Mn^{2+} uptake and accumulation within the cerebellar cortex, while the interior non-enhancing areas refer to white matter. The underlying differences in cell density of the identified layers are in line with recent results obtained by magnetization transfer MRI of mouse cerebellum.[9]

The kinetic behavior of Mn^{2+}-induced MRI signal enhancements after subcutaneous administration is summarized in Table 3 and visualized in Fig. 7. It is characterized by a pronounced and relatively fast MRI signal increase in endocrine tissue without a BBB, and a weaker and delayed enhancement in brain tissues comprising the cerebellum, olfactory bulb and hippocampal CA3 region. The prolonged signal increase of the anterior pituitary gland indicates retention of Mn^{2+} in line with a special uptake mechanism reported for its Ca^{2+} channels.[28]

At 48 h after subcutaneous $MnCl_2$, Fig. 8 shows marked Mn^{2+}-induced MRI signal enhancements of the olfactory bulb and the lateral olfactory tract, adding further evidence for the uptake of Mn^{2+} by secondary olfactory neurons. The sagittal and coronal sections (top and middle rows of Fig. 8) highlight Mn^{2+} contrast in the inferior colliculus, the habenulae on both sides, and the hippocampal formation. Magnified views of a hippocampal ventral section (bottom) reveal a close correspondence of enhanced structures to the dentate gyrus and to

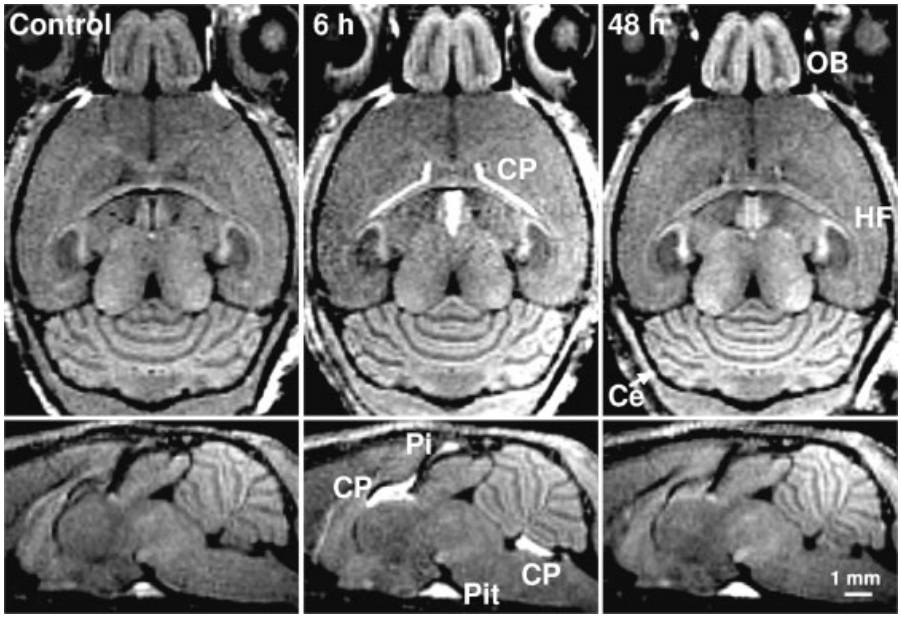

Figure 6. Manganese-induced MRI signal enhancement of the brain of an NMRI mouse (left) before as well as (middle) 6 h and (right) 48 h after subcutaneous injection of 5 ml/kg body weight $MnCl_2$ (20 mM) in (top) horizontal and (bottom) midsagittal sections (T_1-weighted 3D FLASH, $TR/TE = 22/8.2$ ms, 30° flip angle, $120 \times 145 \times 145\ \mu m^3$ interpolated to 120 μm isotropic resolution). In contrast to a marked though transient MRI signal enhancement in the choroid plexus (CP), pineal gland (Pi), and anterior pituitary gland (Pit), brain tissues with a BBB such as the olfactory bulb (OB), dentate gyrus and CA3 subregion of the hippocampal formation (HF), and cerebellum (Ce) exhibit a delayed and more persistent enhancement. [Adapted and reproduced from Watanabe T, Natt O, Boretius S, Frahm J, Michaelis T. *In vivo* 3D MRI staining mouse brain after subcutaneous application of $MnCl_2$. *Magn. Reson. Med*. 2002; **48**: 852–859. Copyright © 2002 John Wiley & Sons, Inc. Reprinted with permission of Wiley-Liss, Inc., a subsidiary of John Wiley & Sons, Inc.][8]

Table 3. SNR of manganese-enhanced structures in NMRI mice after subcutaneous injection of 5 ml/kg body weight $MnCl_2$ (20 mM)

Region	ROI (mm^2)	Control ($n=3$)	6 h ($n=3$)	24 h ($n=4$)	48 h ($n=4$)
Choroid plexus	0.25	28.7 ± 0.8	63.3 ± 1.3*	43.1 ± 6.6*	35.5 ± 1.5*
Pineal gland	0.10	32.3 ± 5.7	57.6 ± 1.0*	36.2 ± 2.5	33.1 ± 1.6
Posterior pituitary	0.13	50.5 ± 2.7	59.3 ± 3.7*	53.0 ± 2.3	54.0 ± 1.3
Anterior pituitary	0.20	37.3 ± 2.1	56.3 ± 7.0*	55.1 ± 5.5*	58.7 ± 5.9*
Frontal cortex	0.26	34.7 ± 0.5	36.2 ± 1.8	35.3 ± 2.9	35.8 ± 2.2
Basal ganglia	0.40	31.1 ± 0.3	33.8 ± 2.2	32.5 ± 3.0	33.5 ± 1.8
Olfactory bulb	2.10	34.5 ± 0.6	39.1 ± 2.2	42.8 ± 4.3*	41.5 ± 2.7*
Olfactory tract	0.10	29.5 ± 0.6	31.3 ± 2.1	36.1 ± 3.4*	37.0 ± 3.0*
Inferior colliculus	0.70	43.7 ± 0.3	43.7 ± 2.3	45.8 ± 5.0	47.8 ± 3.2
Cerebellum	0.50	38.8 ± 0.3	41.5 ± 1.8	42.2 ± 4.5	42.9 ± 2.6*
Hippocampus[a]	0.53	27.4 ± 2.0	32.4 ± 4.5	29.2 ± 1.8	30.4 ± 1.0
CA3	0.15	37.1 ± 1.4	39.5 ± 2.5	40.7 ± 3.7	40.9 ± 2.3*
Dentate gyrus	0.10	37.2 ± 1.5	38.9 ± 2.7	41.0 ± 4.2	42.2 ± 1.3*

The data represent mean values $\pm$ SD averaged across animals; *$p < 0.05$ (unpaired t-test vs control).
[a] Stratum radiatum and stratum lacunosum-moleculare of the Ammon's horn.

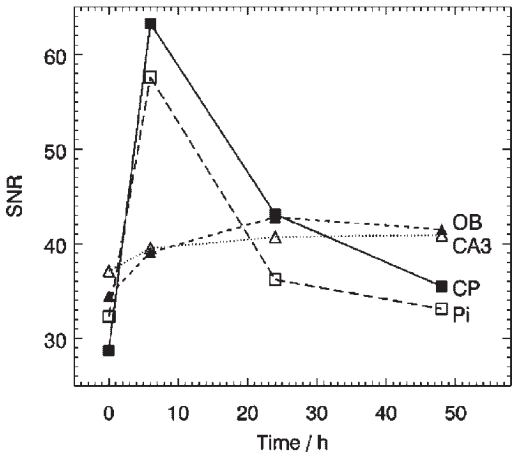

Figure 7. Time course of mean SNR values in selected structures of the brain of NMRI mice before ($n=3$) as well as 6 h ($n=3$), 24 h ($n=4$), and 48 h ($n=4$) after subcutaneous $MnCl_2$ administration. Maximum SNR increases are observed in tissues with a BBB such as the choroid plexus (CP) and pineal gland (Pi). In contrast, crossing of the BBB and neuronal uptake of Mn^{2+} causes a slower and weaker enhancement in the olfactory bulb (OB) and CA3 subregion of the hippocampus. [Adapted and reproduced from Watanabe T, Natt O, Boretius S, Frahm J, Michaelis T. *In vivo* 3D MRI staining mouse brain after subcutaneous application of $MnCl_2$. *Magn. Reson. Med.* 2002; **48**: 852–859. Copyright © 2002 John Wiley & Sons, Inc. Reprinted with permission of Wiley-Liss, Inc., a subsidiary of John Wiley & Sons, Inc.][8]

the CA3 but not CA1 subfield as evidenced by a comparison of pre- and post-contrast images with histology. Thus, the Mn^{2+}-induced contrast in the hippocampal formation most likely originates from the pyramidal cell layer in CA3 as well as from the hilus with parts of the adjacent granule cell layer in the dentate gyrus.

The finding of laminated structures in the mouse cerebellum (Fig. 6) and hippocampal formation (Fig. 8) after $MnCl_2$ administration is in line with similar observations in the rat cortex and olfactory bulb using Mn^{2+}-enhanced MRI.[30] These well-delineated regions are known to consist of sharply defined plexiform layers and cellular layers which often contain the assemblies of large somata. Under these circumstances Mn^{2+} ions become enriched in cellular layers which improves the MRI contrast to neighboring plexiform layers.

MECHANISMS

Uptake of Mn^{2+} into the CNS

The cerebral capillary and the choroid plexus are known to be the two main pathways for Mn^{2+} entry into the CNS.[24] When the plasma concentration of Mn^{2+} increases, the influx of Mn^{2+} into the ventricular CSF is faster than the influx into brain tissue protected by a BBB. In other words, the blood–CSF barrier seems to be more permeable for Mn^{2+} ions than the BBB, so that the uptake into the CNS via the choroid plexus becomes the predominant form.[26] Subsequently, the ependyma, that is the lining of the cerebral ventricles, regulates the transport of ions including Ca^{2+} and Mn^{2+} across the CSF-brain barrier into the interstitial fluid (ISF).[31] Thus, brain regions adjacent to the ventricles may receive significant amounts of Mn^{2+} not only from the cerebral capillaries but also via the ventricular CSF.

Mn^{2+} uptake from the cerebral blood stream via capillary endothelial cells is expected to be largest for neural tissues such as the olfactory bulb and colliculi which contain comparatively large blood volumes.[32,33] Provided that there are no major regional differences in BBB permeability, the higher neuronal availability of Mn^{2+} in these tissues may play a role in the pronounced MRI signal enhancement seen in the olfactory system and in the inferior colliculus after systemic $MnCl_2$

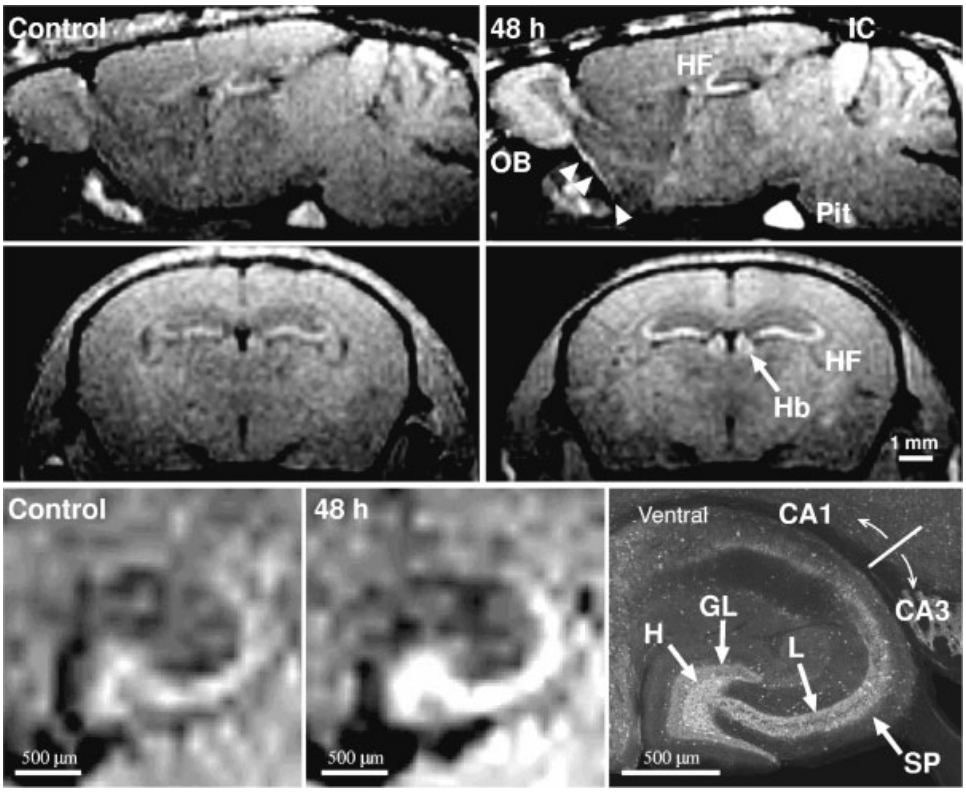

Figure 8. Manganese-induced MRI signal enhancement of the brain of an NMRI mouse before and 48 h after subcutaneous $MnCl_2$ administration in (top) a parasagittal and (middle) a coronal section. Enhanced structures comprise the olfactory bulb (OB), lateral olfactory tract (arrowheads), dentate gyrus and CA3 subregion of the hippocampal formation (HF), inferior colliculus (IC), pituitary lobe (Pit) and habenulae (Hb). (Bottom) Magnified views of a ventral hippocampal section perpendicular to the dorsoventral axis of the hippocampal formation in comparison with histology (courtesy of Jinno *et al.*[29]). The enhancement is most pronounced in the stratum pyramidale (SP) in CA3, stratum lucidum (L), hilus (H), and granule cell layer (GL). For other parameters see Fig. 6. [Adapted and reproduced from Watanabe T, Natt O, Boretius S, Frahm J, Michaelis T. *In vivo* 3D MRI staining mouse brain after subcutaneous application of $MnCl_2$. *Magn. Reson. Med*. 2002; **48**: 852–859. Copyright © 2002 John Wiley & Sons, Inc. Reprinted with permission of Wiley-Liss, Inc., a subsidiary of John Wiley & Sons, Inc.][8]

administration. However, because a strong inflow may also be accompanied by a similar outflow, a blood-pool effect alone cannot account for the retained MRI signal enhancements observed 1–2 days after systemic administration.

Neuronal uptake of Mn^{2+}

Extending *in vitro* studies at the cellular level,[3–5] the present *in vivo* results confirm that extracellular Mn^{2+} ions can enter into neurons via physiologic routes employed for normal brain function. As far as intravitreal injections are concerned, this is supported by the fact that retinal ganglion cells express ion channels that are highly permeable for divalent cations.[34] In the hippocampus both intrahippocampal and systemic administration led to anatomically specific Mn^{2+} enhancements which are in agreement with results obtained by autoradiographic studies.[21] In the absence of major differences in neuroanatomy-both CA1 and CA3 subfields possess the same five-layered cytoarchitecture and contain pyramidal cells as their main neurons-the observed differences in Mn^{2+} enhancement most likely mirror differences in local excitatory connectivity or function. In fact, CA3 and the dentate area represent a prominent example of two reciprocally connected networks[35] in which the recurrent synapses of CA3 have been found to play an essential role in memory acquisition and recall.[36] Moreover, extracellular recordings[37] detected spontaneous action potentials from CA3 but not CA1 pyramidal cell populations, while single-channel recordings[38] indicated that low-voltage-activated Ca^{2+}-channels are particularly abundant on pyramidal neurons in CA3 but not CA1. Thus, the specific Mn^{2+} enhancement in the dentate–CA3 region as opposed to the CA1–subiculum subfields seems to reflect the local functional activity in relation to intrahippocampal processing.

The Mn^{2+}-induced MRI signal enhancements in the olfactory and auditory systems of mice after systemic administration are in agreement with 2-deoxyglucose autoradiograms of rat brain, indicating pronounced activity in structures of the olfactory system[39,40] as well as in the inferior colliculus.[41–43] Thus, the observation of a regional specific Mn^{2+} accumulation may be assumed to reflect, at least in part, integrated regional brain activity in relation to the fact that, in rodents, olfaction and audition are known to dominate perception of the environment under normal circumstances. This situation certainly applies to the mice studied here, which were awake and behaving normally for extended periods of up to 2 days between Mn^{2+} administration and MRI examination.

The affinity of the habenular nucleus to Mn^{2+} enhancement may be related to its unique physiologic properties. Again, 2-deoxyglucose autoradiography clearly demonstrated high levels of metabolic activity for the medial habenular and the interpeduncular nuclei, even during general anesthesia.[44,45] More recently, it has also been observed that the P2X receptor-mediated excitatory postsynaptic currents carried by Ca^{2+} are large within the medial habenula.[46,47]

In general, further uptake mechanisms have to be considered which may result in a slow transfer of Mn^{2+} ions from the extracellular space to intraneuronal compartments.[48] Possible routes not mentioned so far may be due to endocytosis or carrier-mediated transport. It is noteworthy that, the later MRI measurements are performed after Mn^{2+} administration, the more such mechanisms will contribute to the cerebral accumulation.

Axonal transport of Mn^{2+}

Representing a continuous flow of ions and proteins along nerve fibers,[49,50]axonal transport is another physiological process which supports the cerebral distribution of Mn^{2+} subsequent to neuronal uptake. Although the velocity of about 2.8 mm h^{-1} estimated for the progressive Mn^{2+} enhancement from the retina to the superior colliculus includes both the uptake of Mn^{2+} by the retinal ganglion cells and the subsequent flow along the optic nerve and tract, its value is within the range of neuroaxonal transport velocities of about 2 mm h^{-1} obtained for optic nerve fibers in mice[2] and 2.9 mm h^{-1} reported for primary olfactory neurons in pikes.[51]

Mammalian axons exhibit two major anterograde transport processes which possess a wide gap in speed. Slow axonal transport refers to velocities of 0.01–0.33 mm h^{-1}, while the fast transport yields velocities in the range of 2–16 mm h^{-1}.[52] It may therefore be concluded that the predominant contribution to the axonal transport of Mn^{2+} ions stems from the fast process. The responsible mechanism has previously been ascribed to the movement of membranous organelles along microtubules as, for example, demonstrated in the axons of rat retinal ganglion cells.[52] The MRI results obtained after intrahippocampal injection of $MnCl_2$ confirm this interpretation. The SNR increase observed at the site of the ventral hippocampal commissure, which is 4.3 mm distant from the injection site in the posterior hippocampal formation, also requires a transport velocity characteristic for the fast process.

Extraneuronal distribution of Mn^{2+}

Despite the fact that neuronal uptake and subsequent axonal transport of Mn^{2+} are likely to represent the major mechanisms responsible for the cerebral pattern of MRI enhancements, additional factors need to be discussed. This is because neurons are not isolated structures but are dependent on their environment for survival and function. In order to accomplish these goals there exists a well-orchestrated range of mechanisms which allow for a molecular exchange of, for example, ions, metabolites and signalling proteins between extracellular and intracellular compartments. In a wider perspective this also includes intercellular communication as well as exposure to CSF flow and cerebral blood flow. The putative significance of these mechanisms for the distribution of Mn^{2+} in the CNS will be discussed below.

Diffusion of Mn^{2+} within the ISF. Subsequent to focal injections, Mn^{2+} ions may freely diffuse within the ISF and lead to 'secondary' brain uptake. For example, after intracerebral injection, Mn^{2+} not only enters neurons in the immediate target region but also distributes into neighboring areas. Accordingly, the temporal and spatial redistribution of the Mn^{2+}-induced MRI signal enhancement after intrahippocampal injection (Fig. 4, top row) is characterized by a pronounced signal decrease in the inner part of the hippocampal formation between 2 and 6 h after injection. This is supposed to occur by Mn^{2+} diffusion within the ISF. Moreover, enhancement of the hippocampal formation and habenulae was observed 2 days after intravitreal injection (Fig. 3). Because a major retinal projection into these regions has not been reported, the enhancement can be interpreted as evidence for the release of Mn^{2+} ions from the retinal axons, the subsequent diffusion within the ISF, and the neuronal uptake into functionally active brain systems.

Distribution of Mn^{2+} via CSF flow. Figure 9 demonstrates the uptake of Mn^{2+} into the CNS after a single $MnCl_2$ injection into the left lateral ventricle of a mouse. Apart from the signal increase of directly adjacent tissue, the resulting Mn^{2+}-induced MRI signal enhancement reflects both the directional CSF flow from the injected lateral ventricle to the third and fourth ventricle and the functional relevance of the specific uptake into the hippocampal formation and beyond. While signal

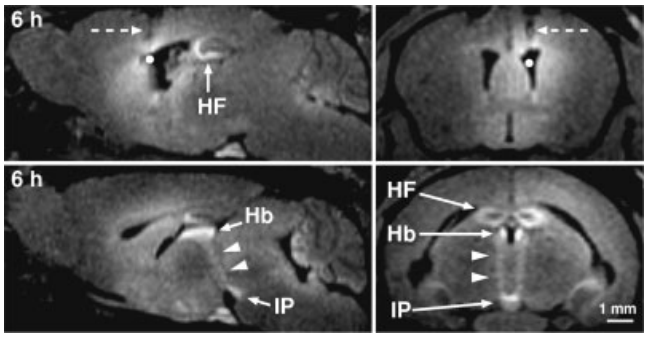

Figure 9. Manganese-induced MRI signal enhancement of the brain of a C57BL/6J mouse 6 h after injection of 0.25 µl of $MnCl_2$ (5 mM) into the left lateral ventricle (T_1-weighted 3D FLASH, *TR/TE* = 17/7.6 ms, 25° flip angle, 117 × 156 × 156 µm^3 interpolated to 117 µm isotropic resolution). (Top left) The injection site (white dots) is depicted in a parasagittal section 0.8 mm lateral to the midline and (top right) in a coronal section with arrows indicating the needle tract. (Bottom left) A parasagittal section 0.35 mm lateral to the midline delineates the connection (arrowheads) between the habenula (Hb) and the interpeduncular nucleus (IP). (Bottom right) An oblique section demonstrates the habenulo–interpeduncular tract (arrowheads) of both sides. Also note that brain tissue adjacent to CSF spaces is highlighted

increases in the hippocampus are more pronounced on the injected side, the enhancement in the habenulae occurs bilaterally. Further on, from the habenulae, enhanced bundles can be traced more ventrally across the thalamus to the interpeduncular nucleus. These observations suggest that the earlier results reported for hippocampal and habenular enhancement after systemic and intravitreal application may be explained, at least in part, by their good accessibility to Mn^{2+} released from CSF-filled spaces. The data are also in line with the aforementioned diffusion of Mn^{2+} ions within the ISF.

Glial uptake of Mn^{2+}. Despite the fact that in brain tissue the uptake and retention of ions occurs preferentially by neurons, this is not an entirely exclusive mechanism as Mn^{2+} ions can also be found in glial cells.[53] Although a significant glial uptake would certainly compromise the use of Mn^{2+}-enhanced MRI for neuroaxonal tract tracing, the data obtained so far support the quantitative predominance of a neuronal rather than glial origin. In particular, this applies to the functionally dependent enhancement observed in specific layers of cell bodies, for example in the cerebellum and CA3. In fact, the enhancement of the efferent hippocampal projection pathway provides unambiguous evidence for a neural effect because the underlying axonal transport requires the preceding uptake of Mn^{2+} by hippocampal neurons. Similarly, the concurrent enhancements in the olfactory bulb and lateral olfactory tract may be treated as another example of the involvement of a cell body assembly together with its major projection pathway. Conversely, a major unspecific uptake of Mn^{2+} in glia would be expected to lead to an even distribution across brain tissues and a homogeneous 'background' MRI enhancement beyond the values observed for control regions in Tables 2 and 3.

Other aspects. When free Mn^{2+} ions enter the intracellular compartment, they bind to intracellular proteins or organelles. This effect has been reported to greatly enhance the intracellular proton relaxivity.[54] In fact, the relaxation dispersion profiles of water protons in solutions containing a variety of Mn^{2+} protein complexes exhibit a maximum in the range of 10–100 MHz.[55] Because of the binding of Mn^{2+} ions, putative contributions to the MRI signal enhancement may also arise from the distribution of Mn^{2+}-dependent enzymes in the brain such as glutamine synthetase and superoxide dismutase.[26] Glutamine synthetase is an astrocyte-specific protein which contains eight Mn^{2+} ions and accounts for approximately 80% of the total Mn^{2+} in brain.[56] In agreement with the present observation of a pronounced Mn^{2+} effect in the Ammon's horn, CA3 pyramidal cells were found to be strongly immunostained by manganese superoxide dismutase, whereas CA1 pyramidal cells were only weakly reactive.[57] However, it is less likely that such effects play a prominent role in acute studies with applications of high external doses. Finally, apart from direct effects on the detectability of MRI signal enhancements, the toxicity of chronic Mn^{2+} applications is expected to alter the functional responses of behaving animals in the later stages of long-term studies.

FUTURE PERSPECTIVES

As demonstrated here and in other contributions to this issue, the distribution of Mn^{2+} ions in the CNS depends on brain function, the route of administration, and several other physiologic factors which are not always under the control of the investigator. In general, these latter effects may pose limitations that are not specific for the use of Mn^{2+} for tissue staining, but also apply to other tracers commonly in use. In order to confirm the neuroaxonal origin and functional significance of Mn^{2+} as a contrast agent, the *in vivo* findings should be correlated with histology and behavior. Moreover, pharmacologically challenged and genetically modified animals may help to gain further insights into the Mn^{2+}-enhanced brain.

Functional tract tracing *in vivo*

In contrast to artifact-prone T_2*-weighted sequences commonly applied for functional MRI of the human brain, Mn^{2+}-induced contrast allows for high-resolution T_1-weighted 3D MRI acquisitions at superb quality. Such data reveal the true 3D architecture of the brain in a way that cannot be appreciated from a series of conventional

histologic slices. It should also be mentioned that recent advances in morphologic tract tracing using diffusion tensor MRI face major SNR problems when attempting to achieve a sufficiently high resolution for murine brain *in vivo*.[58]

In comparison with invasive methods, a limitation of functional tract tracing by Mn^{2+}-enhanced MRI is the lower sensitivity for small fiber tracts. For example, several retinal fiber tracts known to connect to the nuclei of the accessory optic system, as well as to the lateral geniculate and olivary pretectal nuclei in the ipsilateral brain, were not distinguishable after intravitreal injections. This may be caused by a limited local concentration of Mn^{2+} ions due to an insufficient accumulation in respective neurons or by a low axonal fiber density along the target pathway or both. Previous work indicated that Mn^{2+} uptake into the olfactory epithelium and transfer to the olfactory bulb along the primary olfactory neurons is a saturable process.[59] If this applies to the uptake of Mn^{2+} by the retinal ganglion cells or the transport along their axons, the locally achievable concentration might be the limiting factor for the MRI enhancement.

In line with these considerations is the observation that in spite of an excellent agreement of the *in vivo* findings with previous non-MRI tracing studies of retinogeniculate pathways,[12,13] intravitreal injection did not reveal a transsynaptic connection. Delineation of the visual pathway was confined to regions known to directly project from the retina excluding the optic radiation and visual cortex. This lack of MRI demarcation might be caused by a dilution of Mn^{2+} ions due to the fact that the optic radiation diverges and projects into a large visual cortical area.

Another complication may be caused by a release of Mn^{2+} ions from the retinal axons into the ISF as well as from the systemic circulation following absorption by retinal capillary vessels. In fact, the asymmetrically enhanced hippocampus seen late after intravitreal injection (Fig. 3) can be interpreted as evidence for a release of Mn^{2+} ions from the retinal axons.

In the case of focal intracerebral injections, the approach again delineated only major projection fibers from the hippocampal formation. It must be assumed that large amounts of Mn^{2+} ions may have been washed out from the injection site by diffusion within the extracellular space. In this respect, it should be noted that the use of very high $MnCl_2$ concentrations of up to 1000 mM failed to improve the situation by yielding only stronger but anatomically unspecific enhancements. So far, neither high concentrations (> 200 mM $MnCl_2$) nor long waiting periods (> 24 h) were of advantage for a targeted delineation of white matter tracts.

A future perspective for intracerebral $MnCl_2$ microinjections could emerge from experimental indications that Mn^{2+} accumulation in projection areas may serve as a measure of electrophysiologic, that is functional, activity at the injection site.[60] In the hippocampal system, the incoming projections from the entorhinal cortex to the dentate gyrus are relayed to CA3 and subsequently to CA1 which then projects to the subiculum and back to the entorhinal cortex.[61] Apart from forming a closed circuit, each of the hippocampal subfields, except for the dentate gyrus, also gives rise to extrinsic projections. These connections lend further support to the interpretation that the observed Mn^{2+}-enhanced MRI signals in the fimbria and commissural projections (Fig. 5) can be used as a measure for the activity of hippocampal neurons. Depending on the functional activity within this circuitry, the involvement and concurrent electric excitation of the entire hippocampal network is likely to aggravate the uptake of Mn^{2+} by neurons with extrinsic projections. As a consequence, differences in Mn^{2+} accumulation rates at a terminal field (or intermediate projection site) would represent differences in Mn^{2+} influx as a measure of neural activity at the injection site.

Neurofunctional significance of Mn^{2+}-enhanced MRI

Assuming the opening of neuronal Ca^{2+} channels to be coupled to physiological activity, Mn^{2+}-enhanced MRI not only relates to the local Mn^{2+} concentration but also reflects the degree of integrated functional activity over time-apart from the abundance of respective divalent cation channels. This section adds further experimental evidence in favor of the neurofunctional significance of Mn^{2+}-enhanced MRI from studies using pharmacologically challenged animals.

Figure 10 shows the effect of kainic acid on the observable Mn^{2+} distribution within the hippocampal formation. Peripheral injections of kainate are known to result in a degeneration of hippocampal pyramidal cells associated with glial hypertrophy and proliferation.[62] A direct comparison of *in vivo* T_1-weighted MRI with histologic sections from the same animal [Fig. 10(A)] demonstrates that the excitotoxic neuronal cell death causes marked reductions of the normal T_1 contrast in the hippocampal formation yielding only mild to moderate signal intensities. Thus, the pronounced Mn^{2+}-induced signal enhancement in the dentate gyrus and CA3 of controls after subcutaneous administration [Fig. 10(B), upper row] must be assigned to the uptake of Mn^{2+} into functioning hippocampal neurons. In the lesioned animal [Fig. 10(B), bottom row], the residual weak enhancement is more diffuse and slightly shifted across the border of the CA3 region. Under these circumstances one may speculate whether Mn^{2+} is not only taken up by residual viable hippocampal neurons but also by activated glial cells.

Another way of demonstrating synaptic transmission to be a prerequisite for Mn^{2+}-induced MRI signal enhancement is based on a pharmacologic disruption of normal cellular function by blocking the NMDA-type glutamate receptors with the antagonist APV (DL-2-amino-5-phosphonovaleric acid). The procedure hampers synaptic

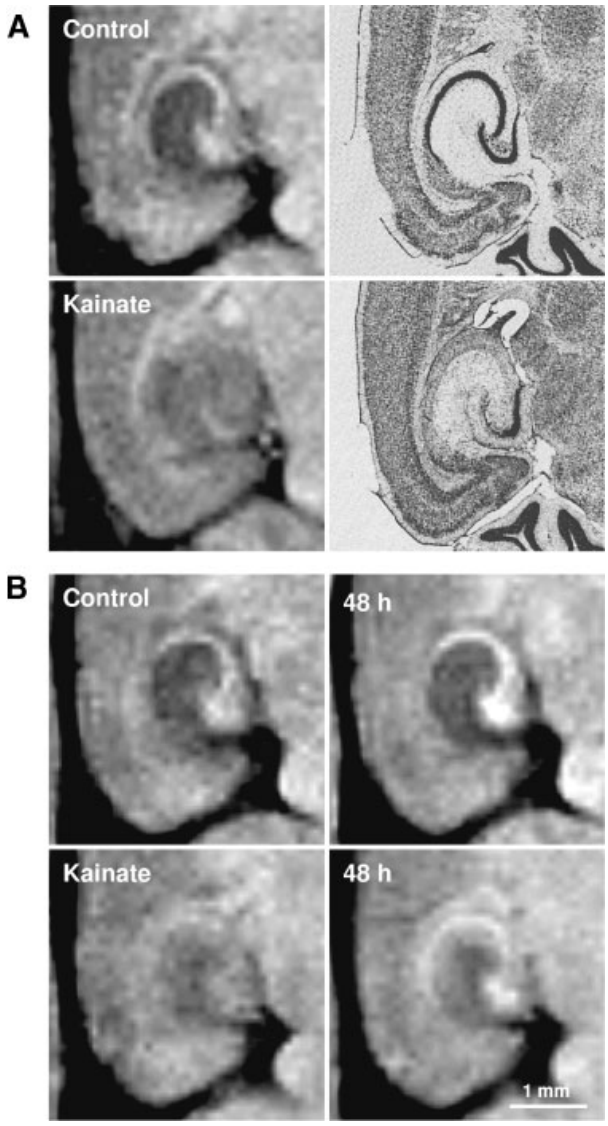

Figure 10. Manganese-induced MRI signal enhancement and kainate-lesioning of the hippocampal formation of FVB/N mice in magnified views of horizontal sections covering the right hippocampus (T_1-weighted 3D FLASH, $TR/TE = 22/8.2$ ms, 30° flip angle, $100 \times 100\,\mu m^2$ in-plane resolution, 500 μm section thickness). (A) Comparison of (left) MRI and (right) Nissl-stained histologic sections 4 days after administration of (top) placebo and (bottom) kainic acid. The pyramidal cell loss in the lesioned animal corresponds to the lack of T_1-weighted MRI signal intensity. Modified from Natt *et al.*[9] (B) Manganese-induced MRI signal enhancement (left) before and (right) 48 h after subcutaneous injection of 5 ml/kg body weight $MnCl_2$ (20 mM) in animals 8 days after administration of (top) placebo and (bottom) kainic acid. In contrast to controls, Mn^{2+} administration in lesioned animals results in only minor to moderate MRI signal increases in the dentate gyrus and outer layers of the Ammon's horn

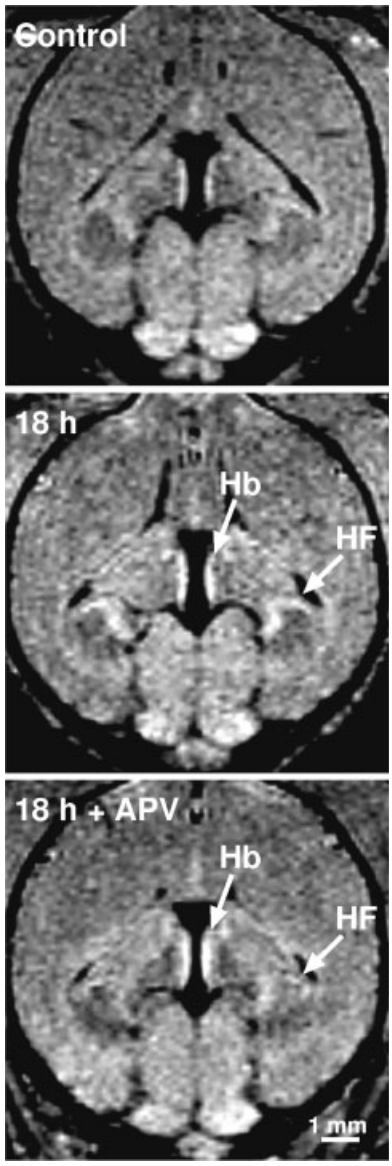

Figure 11. Manganese-induced MRI signal enhancement of the brain of a C57BL/6J mouse (top) before and (middle) 18 h after subcutaneous injection of 5 ml/kg body weight $MnCl_2$ (20 mM) in an oblique section including the dorsal hippocampus and habenulae (T_1-weighted 3D FLASH, $TR/TE = 17/7.6$ ms, 25° flip angle, $117 \times 156 \times 156\,\mu m^3$ interpolated to 117 μm isotropic resolution). (Bottom) Similar acquisitions for a different animal 18 h after subcutaneous injection of $MnCl_2$ and simultaneous intrahippocampal injection of DL-2-amino-5-phosphonovaleric acid (APV, 3.2 μg). Intrahippocampal APV depressed the MRI signal enhancement in the dentate gyrus and CA3 subregion of the hippocampus (HF), but did not alter the enhancement in the habenulae (Hb)

transmission but in contrast to kainate lesioning leaves the morphology of neurons intact. Figure 11 shows preliminary results of bilateral APV injections (3.2 μg dissolved in 0.25 μl artificial CSF) into the posterior hippocampal formation of a C57BL/6J mouse. The procedure followed earlier applications of intrahippocampal $MnCl_2$ and is supposed to minimize mechanical damage to the hippocampal neurons.[10] Immediately after APV administration, the animal received a subcutaneous dose of $MnCl_2$. In comparison with a control (Fig. 11, top and

middle) 3D MRI after 18 h revealed a depression of the otherwise pronounced enhancement in the dentate–CA3 region of the dorsal hippocampus by APV. However, APV did not alter the enhancement in the habenulae which excludes an insufficient delivery of Mn^{2+} to the brain tissue and thus a decreased Mn^{2+} availability for neuronal uptake as an explanation for the lack of enhancement in the hippocampal formation. These findings clearly indicate that other factors than the mere presence of Mn^{2+} in the ISF are responsible for the hippocampal enhancement, namely normal physiologic functioning and neural processing of the cell assemblies in the dentate–CA3 region.

CONCLUDING REMARKS

Manganese may be used as a functional tracer for high-resolution MRI of the rodent brain *in vivo*. Regardless of the route of administration, the observed Mn^{2+} enhancement refers in part to the anatomical distribution of excitatory cells and/or their divalent cation channels, but mainly reflects the functional responses of specific brain systems in terms of neural processing. This involves the intracellular uptake of Mn^{2+} into neurons and subsequent tracing of respective axonal projections. It is foreseeable that the unique insights of Mn^{2+}-enhanced MRI into the functioning brain will open new research opportunities for studying transgenic animals, models of human brain disorders, and novel therapeutic regimens.

Acknowledgments

The authors would like to thank Dr Jelena Radulovic for stereotaxic intracerebral injections, Stefanie Gleisberg for the preparation of histologic sections and Dr Shozo Jinno for providing confocal laser microscopic images.

REFERENCES

1. Lin YJ, Koretsky AP. Manganese ion enhances T_1-weighted MRI during brain activation: an approach to direct imaging of brain function. *Magn. Reson. Med.* 1997; **38**: 378–388.
2. Pautler RG, Silva AC, Koretsky AP. *In vivo* neuronal tract tracing using manganese-enhanced magnetic resonance imaging. *Magn. Reson. Med.* 1998; **40**: 740–748.
3. Drapeau P, Nachshen DA. Manganese fluxes and manganese-dependent neurotransmitter release in presynaptic nerve endings isolated from rat brain. *J. Physiol.* 1984; **348**: 493–510.
4. Narita K, Kawasaki F, Kita H. Mn and Mg influxes through Ca channels of motor nerve terminals are prevented by verapamil in frogs. *Brain Res.* 1990; **510**: 289–295.
5. Simpson PB, Challiss RA, Nahorski SR. Divalent cation entry in cultured rat cerebellar granule cells measured using Mn^{2+} quench of fura 2 fluorescence. *Eur. J. Neurosci.* 1995; **7**: 831–840.
6. Natt O, Watanabe T, Boretius S, Radulovic J, Frahm J, Michaelis T. High-resolution 3D MRI of mouse brain reveals small cerebral structures *in vivo*. *J. Neurosci. Meth.* 2002; **120**: 203–209.
7. Watanabe T, Michaelis T, Frahm J. Mapping of retinal projections in the living rat using high-resolution 3D gradient-echo MRI with Mn^{2+}-induced contrast. *Magn. Reson. Med.* 2001; **46**: 424–429.
8. Watanabe T, Natt O, Boretius S, Frahm J, Michaelis T. *In vivo* 3D MRI staining of mouse brain after subcutaneous application of $MnCl_2$. *Magn. Reson. Med.* 2002; **48**: 852–859.
9. Natt O, Watanabe T, Boretius S, Frahm J, Michaelis T. Magnetization transfer MRI of mouse brain reveals areas of high neural density. *Magn. Reson. Imaging* 2003; **21**: 1113–1120.
10. Watanabe T, Radulovic J, Spiess J, Natt O, Boretius S, Frahm J, Michaelis T. *In vivo* 3D MRI staining of the mouse hippocampal system using intracerebral injection of $MnCl_2$. *Neuroimage* 2004; **22**: 860–867.
11. Voogd J. Visual system. In *The Central Nervous System of Vertebrates*, Nieuwenhuys R, Ten Donkelaar HJ, Nicholson C (eds). Springer: Heidelberg, 1998; 1791–1820.
12. Hayhow WR, Sefton A, Webb C. Primary optic centers of the rat in relation to the terminal distribution of the crossed and uncrossed optic nerve fibers. *J. Comp. Neurol.* 1962; **118**: 295–321.
13. Toga AW, Collins RC. Metabolic response of optic centers to visual stimuli in the albino rat: anatomical and physiological considerations. *J. Comp. Neurol.* 1981; **199**: 443–464.
14. Moore RY, Lenn NJ. A retinohypothalamic projection in the rat. *J. Comp. Neurol.* 1972; **146**: 1–14.
15. Johnson RF, Morin LP, Moore RF. Retinohypothalamic projections in the hamster and rat demonstrated using cholera toxin. *Brain Res.* 1988; **462**: 301–312.
16. Rosene DL, Van Hoesen GW. The hippocampal formation of the primate brain. In *Cerebral Cortex*, Vol. 6, Jones EG, Peters A (eds). Plenum Press: New York, 1987; 345–456.
17. Eichenbaum H. A cortical-hippocampal system for declarative memory. *Nat. Rev. Neurosci.* 2000; **1**: 41–50.
18. Chronister RB, White LE. Fiber architecture of the hippocampal formation: anatomy, projections, and structural significance. In *Hippocampus*, Isaacson RL, Pribram KH (eds). Plenum Press: New York, 1975; 9–31.
19. Rosen GD, Williams AG, Capra JA, Connoly MT, Cruz B, Lu L, Airey DC, Kulkarni K, Williams RW. The mouse brain library @ www.mbl.org. *Int. Mouse Genome Conf.* 2000; **14**: 166.
20. Meibach RC, Siegel A. Efferent connections of the hippocampal formation in the rat. *Brain Res.* 1977; **124**: 197–224.
21. Takeda A, Akiyama T, Sawashita J, Okada S. Brain uptake of trace metals, zinc and manganese, in rats. *Brain Res.* 1994; **640**: 341–344.
22. Takeda A, Ishiwatari S, Okada S. *In vivo* stimulation-induced release of manganese in rat amygdala. *Brain Res.* 1998; **811**: 147–151.
23. Gallez B, Baudelet C, Geurts M. Regional distribution of manganese found in the brain after injection of a single dose of manganese-based contrast agents. *Magn. Reson. Imag.* 1998; **16**: 1211–1215.
24. Murphy VA, Wadhwani KC, Smith QR, Rapoport SI. Saturable transport of manganese(II) across the rat blood-brain barrier. *J. Neurochem.* 1991; **57**: 948–954.
25. Rabin O, Hegedus L, Bourre JM, Smith QR. Rapid brain uptake of manganese(II) across the blood-brain barrier. *J. Neurochem.* 1993; **61**: 509–517.
26. Aschner M. Manganese homeostasis in the CNS. *Environ. Res. A* 1999; **80**: 105–109.
27. Bertinchamps AJ, Miller ST, Cotzias GC. Interdependence of routes excreting manganese. *Am. J. Physiol.* 1966; **211**: 217–224.
28. Cui ZJ, Dannies PS. Thyrotropin-releasing hormone mediated Mn^{2+} entry in perfused rat anterior pituitary cells. *Biochem. J.* 1992; **283**: 507–513.
29. Jinno S, Aika Y, Fukuda T, Kosaka K. Quantitative analysis of GABAergic neurons in mouse hippocampus with optical disector using confocal laser scanning microscopy. *Brain Res.* 1998; **814**: 55–70.
30. Aoki I, Wu YJ, Silva AC, Koretsky AP. Cortical layers revealed by manganese enhanced magnetic resonance imaging (MEMRI) in the rat brain after systemic administration. *Proc. Int. Soc. Magn. Reson. Med.* 2002; **10**: 715.
31. Bruni JE. Ependymal development, proliferation, and functions: a review. *Microsc. Res. Tech.* 1998; **41**: 2–13.
32. Smith QR, Rapoport SI. Cerebrovascular permeability coeffcients to sodium, potassium, and chloride. *J. Neurochem.* 1986; **46**: 1732–1742.

33. Tai C, Smith QR, Rapoport SI. Calcium influxes into brain and cerebrospinal fluid are linearly related to plasma ionized calcium concentration. *Brain Res.* 1986; **385**: 227–236.
34. Taschenberger H, Jüttner R, Grantyn R. Ca^{2+}-permeable P2X receptor channels in cultured rat retinal ganglion cells. *J. Neurosci.* 1999; **19**: 3353–3366.
35. Lisman JE. Relating hippocampal circuitry to function: recall of memory sequences by reciprocal dentate–CA3 interactions. *Neuron* 1999; **22**: 233–242.
36. Tonegawa S, Nakazawa K, Wilson MA. Genetic neuroscience of mammalian learning and memory. *Phil. Trans. R. Soc. Lond. B* 2003; **358**: 787–795.
37. Cohen I, Miles R. Contributions of intrinsic and synaptic activities to the generation of neuronal discharges in *in vitro* hippocampus. *J. Physiol. (Lond.)* 2000; **524**: 485–502.
38. Fisher RE, Gray R, Johnston D. Properties and distribution of single voltage-gated calcium channels in adult hippocampal neurons. *J. Neurophysiol.* 1990; **64**: 91–104.
39. Schwartz WJ, Sharp FR. Autoradiographic maps of regional brain glucose consumption in resting, awake rats using [^{14}C]2-deoxyglucose. *J. Comp. Neurol.* 1978; **177**: 335–360.
40. Astic L, Saucier D. Metabolic mapping of functional activity in the olfactory projections of the rat: ontogenetic study. *Dev. Brain Res.* 1982; **2**: 141–156.
41. Sokoloff L, Reivich M, Kennedy C, Des Rosiers MH, Patlak CS, Pettigrew KD, Sakurada O, Shinohara M. The [^{14}C]deoxyglucose method for the measurement of local cerebral glucose utilization: theory procedure, and anesthetized albino rat. *J. Neurochem.* 1977; **28**: 897–916.
42. Nelson SR, Howard RB, Cross RS, Samson F. Ketamine-induced changes in regional glucose utilization in the rat brain. *Anesthesiology* 1980; **52**: 330–334.
43. Duncan GE, Miyamoto S, Leipzig JN, Lieberman JA. Comparison of brain metabolic activity patterns induced by ketamine, MK-801 and amphetamine in rats: support for NMDA receptor involvement in responses to subanesthetic dose of ketamine. *Brain Res.* 1999; **843**: 171–183.
44. Herkenham M. Anesthetics and the habenulo-interpeduncular system: selective sparing of metabolic activity. *Brain Res.* 1981; **210**: 461–466.
45. McQueen JK, Martin MJ, Harmar AJ. Local changes in cerebral 2-deoxyglucose uptake during alphaxalone anaesthesia with special reference to the habenulo-interpeduncular system. *Brain Res.* 1984; **300**: 19–26.
46. Edwards FA, Robertson SJ, Gibb AJ. Properties of ATP receptor-mediated synaptic transmission in the rat medial habenula. *Neuropharmacology* 1997; **36**: 1253–1268.
47. Khakh BS. Molecular physiology of P2X receptors and ATP signalling at synapses. *Nat. Rev. Neurosci.* 1997; **36**: 1253–1268.
48. Takeda A. Manganese action in brain function. *Brain Res. Rev.* 2003; **41**: 79–87.
49. Taylor AC, Weiss P. Demonstration of axonal flow by the movement of tritium-labeled protein in mature optic nerve fibers. *Proc. Natl Acad. Sci. USA* 1965; **54**: 1521–1527.
50. Goldstein LSB, Yang Z. Microtubule-based transport systems in neurons: the roles of kinesins and dyneins. *A. Rev. Neurosci.* 2000; **23**: 39–71.
51. Tjälve H, Mejàre C, Borg-Neczak K. Uptake and transport of manganese in primary and secondary olfactory neurones in pike. *Pharmac. Toxicol.* 1995; **77**: 23–31.
52. Elluru RG, Bloom GS, Brady ST. Fast axonal transport of kinesin in the rat visual system: functionality of kinesin heavy chain isoforms. *Mol. Biol. Cell* 1995; **6**: 21–40.
53. Tiffany-Castiglioni E, Qian Y. Astroglia as metal depots: molecular mechanisms for metal accumulation, storage and release. *Neurotoxicology* 2001; **22**: 577–592.
54. Nordhøy W, Anthonsen HW, Bruvold M, Jynge P, Krane J, Brurok H. Manganese ions as intracellular contrast agents: proton relaxation and calcium interactions in rat myocardium. *NMR Biomed.* 2003; **16**: 82–95.
55. Koenig SH, Brown RD. Relaxation of solvent protons by paramagnetic ions and its dependence on magnetic field and chemical environment: implications for NMR imaging. *Magn. Reson. Med.* 1984; **1**: 478–495.
56. Wedler FC, Denman RB. Glutamine synthetase: the major Mn (II) enzyme in mammalian brain. *Curr. Top. Cell. Regul.* 1984; **24**: 153–169.
57. Akai F, Maeda M, Suzuki K, Inagaki S, Takagi H, Taniguchi N. Immunocytochemical localization of manganese superoxide dismutase (Mn-SOD) in the hippocampus of the rat. *Neurosci. Lett.* 1990; **115**: 19–23.
58. Boretius S, Watanabe T, Natt O, Michaelis T, Finsterbusch J, Frahm J. Diffusion tensor mapping of living mouse brain using half-Fourier single-shot STEAM MRI. *Proc. Int. Soc. Magn. Reson. Med.* 2002; **10**: 1231.
59. Henriksson J, Tallkvist J, Tjälve H. Transport of manganese via the olfactory pathway in rats: dosage dependency of the uptake and subcellular distribution of the metal in the olfactory epithelium and the brain. *Toxicol. Appl. Pharmac.* 1999; **156**: 119–128.
60. Tindemans I, Verhoye M, Balthazart J, Van der Linden A. *In vivo* dynamic ME-MRI reveals differential functional responses of RA- and area X-projecting neurons in the HVC of canaries exposed to conspecific song. *Eur. J. Neurosci.* 2003; **18**: 3352–3360.
61. Nieuwenhuys R. Cerebral cortex. In *The Central Nervous System of Vertebrates*, Nieuwenhuys R, Ten Donkelaar HJ, Nicholson C (eds). Springer: Heidelberg, 1998; 1944–1952.
62. Che Y, Yu YM, Han PL, Lee JK. Delayed induction of p38 MAPKs in reactive astrocytes in the brain of mice after KA-induced seizure. *Mol. Brain Res.* 2001; **94**: 157–165.

